

# Nanosecond laser induced damage mechanism of multilayer dielectric gratings

KEPENG WU<sup>a</sup>, ZHILIN XIA<sup>a,\*</sup>, FANYU KONG<sup>b</sup>, YUNXIA JIN<sup>b</sup>

<sup>a</sup>*School of Materials Science and Engineering, Wuhan University of Technology, Wuhan, Hubei 430070, PR China*

<sup>b</sup>*Key Laboratory of Materials for High Power Laser, Shanghai Institute of Optics and Fine Mechanics, Chinese Academy of Sciences, Shanghai 201800, PR China*

A multilayer dielectric grating used for laser pulse compression was designed. The gratings laser damage experiment was also performed. The observed damage morphologies cannot be interpreted only based on the usually used electromagnetic field distribution. Therefore, the temperature and thermal stress field distributions also have been calculated, and the affection of absorbing impurities and defects on the gratings damage process has been analyzed. The damage process happened in experiments is consistent with the theoretical predicted process, which is obtained based on the defects absorption. The absorptive defects are convinced to initialize the gratings damage. Defects located at different sites have different degrees of affection on the surface temperature and thermal stress distributions. Hence, the damage pits were appeared in different stages of laser irradiation and uneven distributed on the gratings surface.

(Received December 1, 2016; accepted June 7, 2018)

*Keywords:* Diffraction gratings, Laser induced damage, Pulse compression

## 1. Introduction

The chirped pulse amplification (CPA) technology is a main approach to achieve high-intensity short-pulse laser. Diffraction gratings are good candidates for stretching and compressing laser pulses in CPA [1-5]. To achieve high intensity laser pulses, the used pulse compression gratings (PCG) must meet the requirements of high diffraction efficiency and high laser damage resistance. The final gratings in the pulse compressor typically need to endure the laser irradiation with the highest power density [6-8]. As the development of PCGs, gold-coated gratings have been gradually replaced by multilayer dielectric gratings (MDGs) because of the inherent absorption of metals [9, 10]. The so-called MDG is composed of a multilayer dielectric mirror and a grating structure. Generally, the -1<sup>st</sup> order diffraction efficiency of a MDG can exceed 96% [9]. To improve the longevity of a pulse laser system, a better understanding of the damage mechanism and constantly improving the laser damage resistance of the MDG should be given more attention.

Impurities and defects are the main damage causes in the case of a laser irradiation with a pulse width from picosecond to nanosecond. The picosecond pulsed laser induced damage of MDGs in high power density laser systems is a key issue and it has been widely studied. Under a laser irradiation with a pulse width of several picosecond, the damage of optical elements is usually dominated by the stress action. If the pulse width is longer

than hundreds of picoseconds, the damage is usually dominated by the thermal action. In the transition region (a pulse width of tens of picoseconds), both stress and thermal processes will happen. The picosecond pulsed laser induced damage mechanisms were usually analyzed based on the stress action. Seldom work is performed to investigate the effect of the heat action on the MDG's damage. In this paper, the heat action caused damage characteristics of MDGs have been studied. In the following, firstly, the experimental damage morphologies have been revealed. Then, the electromagnetic field, temperature field and thermal stress field distributions in an ideal grating structure have been calculated. Lastly, the affection of absorbing impurities and defects on the gratings damage process has been analyzed.

## 2. Experimental sketch and results

The MDG used for laser pulse compression was designed to have a line density of 1740 lines/mm on a dielectric high-reflectivity (HR) mirror. The HR mirror is composed of alternating SiO<sub>2</sub>/HfO<sub>2</sub> layers, and the stack structure is Substrate/(H<sub>2</sub>L)<sup>9</sup>H<sub>3</sub>L/Air, in which H means HfO<sub>2</sub> and L means SiO<sub>2</sub>. The alternating HfO<sub>2</sub> and SiO<sub>2</sub> layers were deposited onto a fused silica substrate via electron beam evaporation. The grating structure was fabricated by ion-beam etching the top layer (SiO<sub>2</sub> layer) of the HR mirror. The structure of each grating pillar is

trapezoidal in shape. The grating layer has a duty cycle of 0.30, a groove depth of 300 nm, and a trapezoid angle of  $80^\circ$ . The  $-1^{\text{st}}$  order diffraction efficiency of well-cleaned samples is greater than 96% at an incident angle of 70 degrees for TE polarized laser light at a wavelength of 1053 nm [11].

The schematic of the damage test setup can be referred in Ref.11. A 1064 nm Nd: YAG laser system

produces a near-Gaussian spatial profile. The effective size of the focused spot is  $0.016 \text{ mm}^2$  in the beam normal. The test conditions of laser damage experiments were selected as follows: the incidence angle is 70 degrees, TE polarization was used, and the pulse width is 12 ns. Every test site was exposed to one pulse. Fig. 1 shows the damage morphologies of a damage spot.

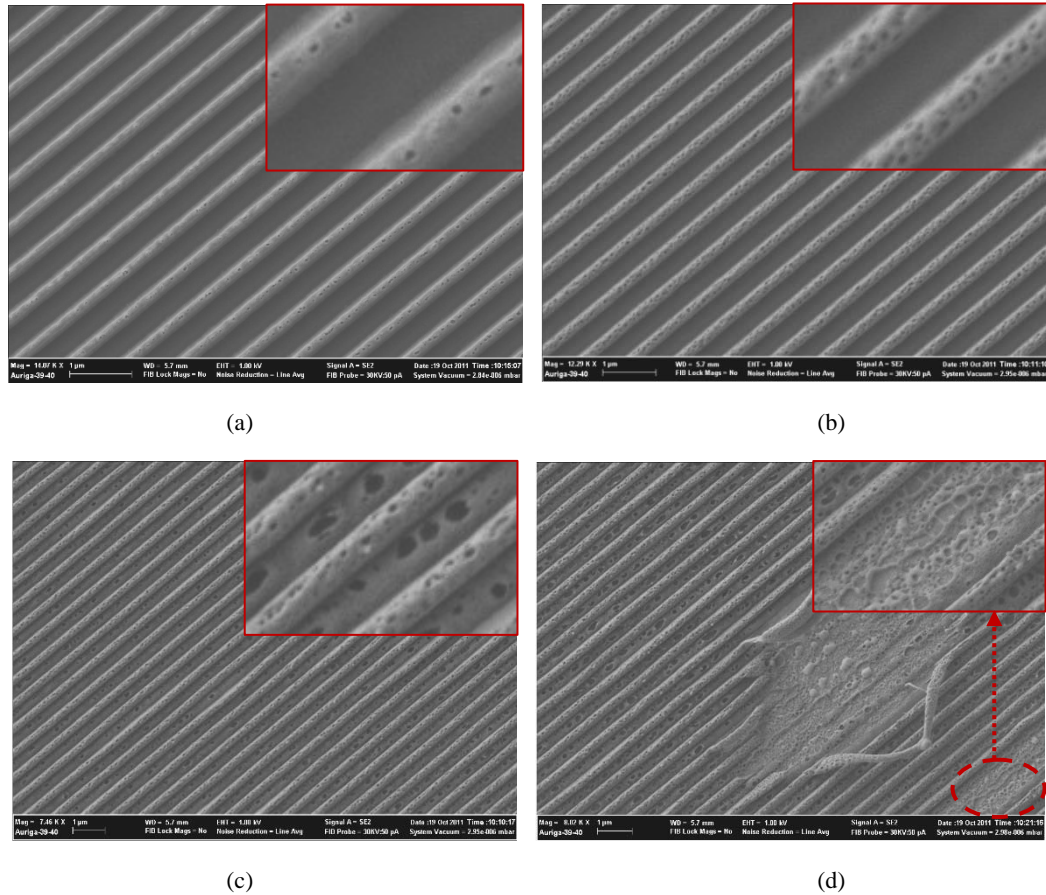


Fig. 1. The damage morphologies of the gratings (the test laser energy density is  $10.1 \text{ J/cm}^2$  and the damage threshold of the sample is  $8.2 \text{ J/cm}^2$ ). (a)~(d) are corresponding to different sites of the damage spot. (a) and (d) display the farthest and the nearest positions from the damage spot center respectively

Fig. 1(a) shows the damage morphology at the edge of the damage spot. It can be seen that many small damage pits appear on grating ridges, and these damage pits are discrete distributed. No damage pits are observed in the groove part. Fig. 1(b) shows the damage morphology at a site closer to the center of the damage spot. It can be seen that the density of damage pits on grating ridges is higher. Damage pits still have not been observed in the groove part. Fig. 1(c) shows the damage morphology at a site further close to the center of the damage spot. It can be seen that the density of damage pits on grating ridges is further high, and damage pits are observed in the groove part. Damage pits in the groove part were uneven distributed and mainly gathered on one side. Some large damage pits are also observed in the groove part. Fig. 1(d) shows the damage morphology near the center of the

damage spot. The grating ridges in some areas were flattened or peeled.

The gratings damage process can be deduced based on the morphology change at different sites of the damage spot. Therefore, the probable laser damage process of the multilayer dielectric gratings is that: some discrete distributed damage pits firstly only appear on grating ridges and the density continuous to grow. After a period of laser irradiation, some damage pits will appear in the groove part, and the distribution is uneven. Some large damage pits will also form in the groove part. In the late stage of the damage development, some grating ridges start lodging and peeling.

The damage pits on gratings surface are discrete distributed. This is the typical characteristic of the absorptive impurities or defects induced damage. If the damage process is not dominated by absorption impurities

or defects, the damage morphology should be a groove on each ridge extending along the direction of grating bars. In the below, absorptive impurities and defects were introduced to analyze the damage characteristics of the prepared gratings.

### 3. Theoretical models and discussions

In the case of nanosecond pulsed laser induced damages of dielectrics, the damage process is usually dominated by thermodynamic actions. Therefore, the electromagnetic field, temperature field and the thermal stress field in the designed gratings have been calculated. Fig. 2 shows the calculated field distributions. The

calculation domain is divided into four layers: the air layer with a thickness of 1200 nm used in calculation; the grating layer and the multi-layer dielectric films (part of it is displayed) with the same structure as that used in experiments; and the substrate layer, which is not revealed in Fig. 2. An S-polarized laser with wavelength of 1064 nm is incident at an incident angle of  $70^\circ$  from the left side in air. The laser irradiation area contains hundreds of grating periods, so periodic boundaries can be used to reduce the computational region. In calculation, the left and right boundaries were periodic boundaries, the surface of the gratings was set as a free and thermal conduction boundary, and the lower boundary of the substrate layer was set as a fixed and thermal radiation boundary. The air layer was not included in thermal stress field calculations.

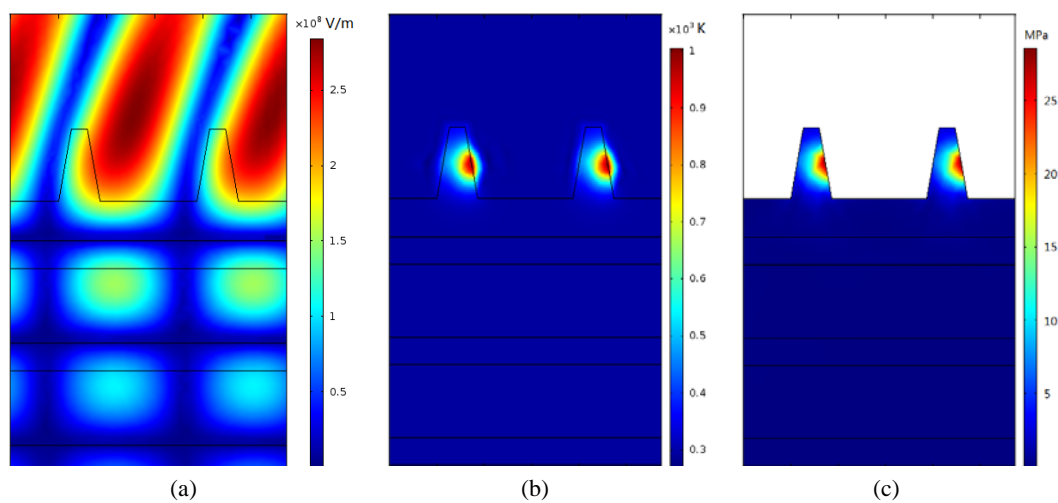


Fig. 2. The calculated electromagnetic field (a), temperature field (b) and thermal stress field (c) distributions in the gratings

The parameters used in calculations are: the laser energy density is  $10 \text{ J/cm}^2$ ; the refractivity of the  $\text{HfO}_2$ ,  $\text{SiO}_2$  and substrate are 1.96, 1.46 and 1.52 respectively; the thermal conductivity of  $\text{HfO}_2$  and  $\text{SiO}_2$  are 2.0 and 1.38 W/m/K respectively; the heat capacity at constant pressure of  $\text{HfO}_2$  and  $\text{SiO}_2$  are 800 and 753 J/Kg/K respectively; the Yong's ratio of  $\text{HfO}_2$  and  $\text{SiO}_2$  are 256 and 72 GPa respectively; the Poisson's ratio of  $\text{HfO}_2$  and  $\text{SiO}_2$  are 0.18 and 0.17 respectively; the coefficient of thermal expansion of  $\text{HfO}_2$  and  $\text{SiO}_2$  are  $0.55 \times 10^{-6}$  and  $5.6 \times 10^{-6}$ /K respectively. The thermodynamic parameters of the substrate are those of the Silica. Considering the laser induced ionization of materials, the extinction coefficient of the surface silica layer is not zero. Besides, the calculation purpose in this paper is not predicting damage threshold but understanding the damage occurrence position, so a not accurate value of 0.0002 was adopt as the extinction coefficient of the surface silica layer.

Furthermore, the Maxwell's equations were used to calculate the electromagnetic field, the Fourier's law of the heat conduction was used to calculate the temperature field and the Hooke's law was used to calculate the thermal

stress field. The finite element method in time domain was used in calculations.

Fig. 2(a) shows the laser electromagnetic field distribution. The laser field is periodically distributed along the direction of the grating alignment. The highest laser intensity locates in the middle part of the ridge site wall, which is back to the incident light. In the basic HR mirror, the laser field is also periodically distributed because of the periodic stack structure. When the laser beam enters the HR mirror, its field strength reduces rapidly. Fig. 2(b) shows the temperature field distribution. Some hot spots are formed in the middle part of the ridge site wall, which is back to the incident light. In the basic HR mirror, the temperature is not high because of the relative low laser field. Fig. 2(c) shows the thermal stress field distribution. The stress distribution has similar characteristics to the temperature distribution.

According to the temperature field and stress field distributions in the gratings with an ideal designed structure, the damage should be firstly appeared in the middle part of ridge site walls, and the damage morphology should be some ablation stripes. More seriously, the grating ridges will be flattened or peeled.

These damage characteristics have been observed in experiments in the late stage of the damage process. However, the damage characteristics in the early stage of the damage process cannot be interpreted. There are some other mechanisms dominated the early stage of the damage process.

Considering the discrete distribution characteristic of the damage pits, some absorptive impurities and defects were introduced, and the temperature as well as thermal stress distributions has been calculated. Two kinds of particles (impurities and defects) have been considered in calculations. One of them is the impurities attached on the gratings surface, and the other one is the defects included in the shallow surface of gratings. In order to analyze the damage occurrence sequence at different positions on gratings surface, particles with the same size has been used in different positions.

Fig. 3 shows the distribution location and the number of the introduced absorptive particles. The particles numbered as 1, 3 and 5 are located in/on the grooves, and the particles numbered as 2, 4 and 6 are located in/on the ridges. Because all impurities and defects are attached to or included in the silica layer, the materials parameters used for impurities and defects are those of the silica except for the refractivity, which is  $1.46 + i \cdot 0.001$ . The extinction coefficient of impurities and defects is larger than that of the pure silica, because impurities and defects usually have a stronger absorptive capacity. The calculated electromagnetic field in gratings with impurities and defects is similar to that of gratings with an ideal structure. This is because that the impurity and defect size is less than the incident light wavelength and no obvious scattering will be caused by impurities and defects. According to the size of damage pits shown in Fig. 1, the impurity and defect size should be smaller than 50 nm. For comparison, impurities and defects with the same size were used and their diameter is 40 nm.

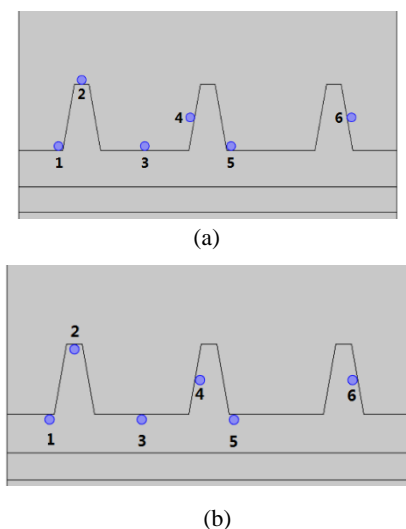


Fig. 3. The calculation model of gratings with absorptive particles. (a) the impurities attached on the surface (b) the defects included in the shallow surface

Fig. 4 gives the temperature distribution in gratings with impurities and defects. It can be seen that the maximal temperature locates in particles numbered as 6. Particles numbered as 1 has little effect on the temperature field distribution. For particles numbered as 2 and 4, the laser intensity in the attached impurities is less than that in the included defects. The lower laser intensity corresponds to the lower temperature. Similarly, for the particles numbered as 3, 5 and 6, the temperature in the attached impurities is higher than that of the included defects. Besides, for the impurities attached on the surface, it can be seen from Fig. 4 (a) that the absorbed energy is mainly deposited in the impurity itself, and the heat-affected region around the impurity is very small because of the small thermal diffusion coefficient of air. While for the defects included in gratings, as Fig. 4 (b) shows, the heat-affected region around the defect is larger.

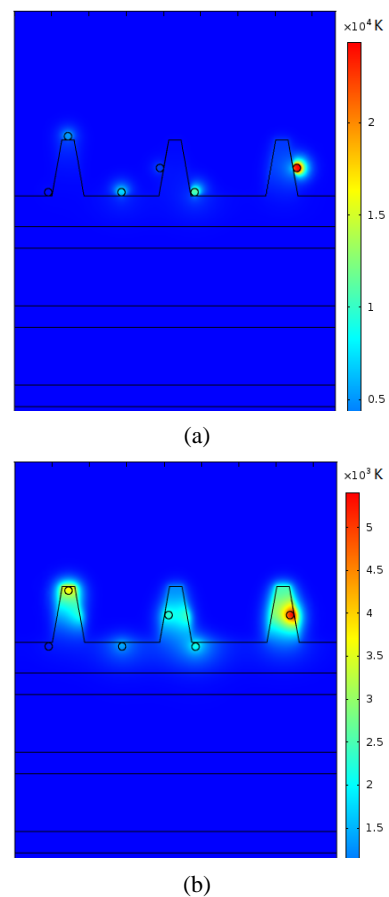


Fig. 4. The temperature distributions in gratings with absorptive particles. (a) the impurities attached on the surface (b) the defects included in the shallow surface

Fig. 5 gives the gratings surface temperature and thermal stress distribution curves. The ridge-groove junctions are identified by some arrows near the horizontal axis in Fig. 5(b). The stress concentrations at these sites are caused by the grating structure, and have nothing to do with the particles.

In Fig. 5, the relative temperatures and thermal stresses near different particles are more meaningful than the absolute values. According to the relative temperatures and thermal stresses, the damage occurrence sequence near different particles can be judged. Near the particle numbered as 6, whether it is included in or attached on gratings surface, the gratings surface temperature and thermal stress are the highest. Accordingly, the damage firstly happens on grating ridges.

If damage pits were initialized by attached impurities, according to the relative values of the temperature and stress from high to low, the corresponding damage sequence is 6, 5, 3, 2, 4 and 1. Particles numbered as 1 and 4 have little impact on the field distributions. The damage process should be that: some discrete distributed damage pits firstly only appear on grating ridges. Then the some damage pits will appear in the groove part and the density continuous to grow. Subsequently, the density of damage pits appeared on grating ridges will increase. This damage process is not consistent with the experimental observed phenomenon.

If damage pits were initialized by included defects and attached impurities, the sequence is the same as that initialized only by attached impurities. Therefore, attached impurities have little contribution to the formation of damage pits.

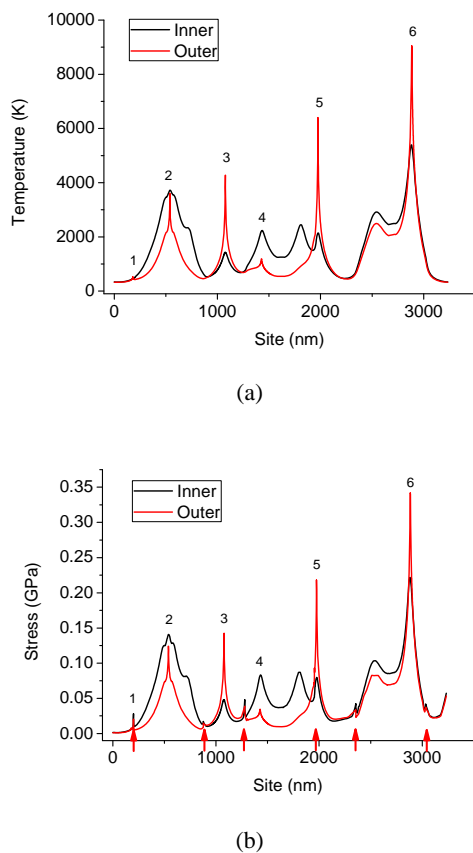


Fig. 5. The surface temperature and thermal stress distributions of gratings with absorptive particles. (a) the surface temperature distribution (b) the surface thermal stress distribution

If damage pits were initialized by included defects, according to the relative values of the temperature and stress from high to low, the corresponding damage sequence is 6, 2, 4, 5, 3 and 1. This sequence is consistent with the experimental observed phenomenon. Therefore, the damage pits appeared on the gratings surface were likely to be caused by the included defects. These defects were probably formed during the course of etching grating structure by the high current ion beam.

Besides, as for included defects numbered as 1, 3 and 5, the temperature and stress near defects numbered as 5 is the highest. Defects numbered as 1 has little effect on the field distributions. Hence, the damage pits in the groove part will be concentrated near the junction region, which is back to the incident light. This is also consistent with the experimental observed phenomenon.

#### 4. Conclusions

The damage process of multilayer dielectric gratings designed in this paper induced by thermal ablations is that some discrete distributed damage pits firstly only appear on grating ridges. After a period of laser irradiation, some damage pits will appear in the groove part with an uneven distribution. In the late stage of the damage development, some ridges start lodging and peeling. This damage process is not consistent with the theoretical process obtained based on the attached impurities absorption, but consistent with the theoretical process obtained based on the included defects absorption. The damage pits formed on gratings surface could be caused by the included defects. As for defects in the groove part, the surface temperature near the junction region, which is back to the incident light, is the highest. Hence, the damages in the groove part are concentrated in this side. The conclusions in this paper is help for understanding the thermal process, which may happens in the case of picosecond pulsed laser induced MDG's damage. In this calculation, the used diameters of impurities and defects are the same. The influence of defect size on damage pits has not been considered. The size of heat-affected zones near impurities and defects cannot be used to analyze the damage formation mechanisms.

#### Acknowledgments

The work was supported by NSAF (No. U1430121). The authors gratefully acknowledge the financial support of the National Science Foundation of China (Grant 10704079), and the Open Research Fund of Key Laboratory of Material for High Power Lasers - Chinese Academy of Sciences.

**References**

- [1] D. Strickland, G. Mourou, *Opt. Comm.* **56**, 219 (1985).
- [2] H. Guan, H. Chen, J. Wu, Y. Jin, F. Kong, S. Liu, K. Yi, J. Shao, *Opt. Lett.* **39**, 170 (2014).
- [3] M. Rumpel, M. Moeller, C. Moormann, T. Graf, A. M. Abdou, *Opt. Lett.* **39**, 323 (2014).
- [4] S. Palmier, J. Neauport, N. Baclet, *Opt. Express* **17**, 20430 (2009).
- [5] P. Poole, S. Trendafilov, G. Shvets, D. Smith, E. Chowdhury, *Opt. Express* **21**, 26341 (2013).
- [6] J. Neauport, N. Bonod, S. Hocquet, S. Palmier, G. Dupuy, *Opt. Express* **18**, 23776 (2010).
- [7] Y. Du, X. Wu, M. Zhu, Z. Le, *Opt. Express* **23**, 24296 (2015).
- [8] K. He, J. Wang, Y. Hou, X. Li, H. Guan, F. Kong, S. Liu, Y. Jin, K. Yi, *Appl. Opt.* **52**, 653 (2013).
- [9] M. D. Perry, R. D. Boyd, J. A. Britten, D. Decker, B. W. Shore, C. Shannon, E. Shults, *Opt. Lett.* **20**, 940 (1995).
- [10] B. W. Shore, M. D. Perry, J. A. Britten, R. D. Boyd, M. D. Feit, H. T. Nguyen, R. Chow, G. E. Loomis, L. Li. *J. Opt. Soc. Am. A* **14**, 1124 (1997).
- [11] Z. L. Xia, D. W. Li, Y. A. Zhao, Y. T. Wu, *Opt. Laser Technol.* **46**, 77 (2013).

---

\*Corresponding author: xiazhilin@whut.edu.cn